



## Supporting Information

for *Adv. Sci.*, DOI: 10.1002/advs.202103826

### In situ Formed Ag-Li Intermetallic Layer for Stable Cycling of All-solid-state Lithium Batteries

*Hong Jun Choi, Dong Woo Kang, Jun-Woo Park, Jun-Ho Park, Yoo-Jun Lee, Yoon-Cheol Ha, Sang-Min Lee, Seog Young Yoon\*, and Byung Gon Kim\**

## Supporting Information

**In situ Formed Ag-Li Intermetallic Layer for Stable Cycling of All-solid-state Lithium Batteries**

*Hong Jun Choi, Dong Woo Kang, Jun-Woo Park, Jun-Ho Park, Yoo-Jun Lee, Yoon-Cheol Ha, Sang-Min Lee, Seog Young Yoon\*, and Byung Gon Kim\**

H. J. Choi, D. W. Kang, Dr. J.-W. Park, Dr. Y.-J. Lee, Dr. Y.-C. Ha, Dr. S.-M. Lee,<sup>[†]</sup> Dr. B. G. Kim

Next Generation Battery Research Center, Korea Electrotechnology Research Institute (KERI), 12, Jeongiui-gil, Seongsan-gu, Changwon-si, Gyeongsangnam-do 51543, Republic of Korea

E-mail: byunggonkim@keri.re.kr

H. J. Choi, Prof. S. Y. Yoon

School of Materials Science and Engineering, Pusan National University, 2, Busandaehak-ro 63beon-gil, Geumjeong-gu, Busan, 46241, Republic of Korea

E-mail: syy3@pusan.ac.kr

<sup>[†]</sup>Present address: Graduate Institute of Ferrous & Energy Materials Technology, Pohang University of Science and Technology (POSTECH), 77 Cheongam-Ro, Nam-gu, Pohang, Gyeongbuk 37673, Republic of Korea

## Experimental Section

*Materials:* Ag foil (thickness = 10  $\mu\text{m}$ , 99.98%) was purchased from Nilaco (Japan). Li metal foil (thickness = 40, 150, and 250  $\mu\text{m}$ ) was purchased from Honjo (Japan). Stainless steel foil (SS, thickness = 10  $\mu\text{m}$ ) was purchased from MTI Korea (Korea).  $\text{Li}_2\text{S}$  (99.98%),  $\text{P}_2\text{S}_5$  (99%), and  $\text{LiCl}$  (99%) were purchased from Sigma-Aldrich (USA).  $\text{LiNi}_{0.6}\text{Co}_{0.2}\text{Mn}_{0.2}\text{O}_2$  (NCM, particle diameter: 4  $\mu\text{m}$ ) was provided by the L&F Co. (Korea). Graphitic hollow nanocarbon (GHC) was obtained using heat treatment of Super P (TIMCAL, Switzerland) at 2400  $^\circ\text{C}$ .<sup>[S1]</sup> In this study, the GHC was used as a conducting agent because it can mitigate the interfacial side reactions between the solid electrolyte (SE) and additive.

*Preparation of Ag-Li Alloy and LPSCl Solid Electrolyte:* The Ag-Li alloy foil was prepared by roll pressing using Ag and Li foils, and the as-prepared foil was kept under external pressure to complete the Ag-Li alloying reaction using a jig for 2 days. The sulfide SE, argyrodite  $\text{Li}_6\text{PS}_5\text{Cl}$  (LPSCl), was prepared based on the following procedure.<sup>[S2,S3]</sup> A stoichiometric mixture of  $\text{Li}_2\text{S}$ ,  $\text{P}_2\text{S}_5$ , and  $\text{LiCl}$  was mechanically ball-milled at 600 rpm for 10 h using a high energy ball-milling machine (Pulverizett7, Fritsch, USA). After finishing the milling process, the vessel was transferred into a glove box, and the LPSCl powder was obtained.

*Test Cell Assembly and Electrochemical Tests:* Prior to preparing the composite cathode, all materials were dried under vacuum at 80  $^\circ\text{C}$  overnight, and then, transferred into an Ar-filled glovebox. To obtain a homogeneous mixture, the composite cathode was prepared by hand-mixing the NCM cathode material, LPSCl solid electrolyte, and GHC conducting agent in a weight ratio of 75:23:2, using an agate mortar for 40 min. To test the electrochemical performance, the homemade pressurized cell was assembled.<sup>[S1,S4]</sup> First, 200 mg of the SE was placed in the polyether ether ketone mold (diameter: 14 mm) and cold pressed with 0.5 ton for 1 min. Then, 26.7 or 49.3 mg (loading: 13 or 24  $\text{mg}_{\text{NCM}} \text{cm}^{-2}$ , areal capacity: 2.3 or 4.3  $\text{mAh cm}^{-2}$ ) of cathode composite was filled on the SE pellet and cold pressed with 4 tons for 3 min.

The Ag-Li alloyed foil with an SS current collector was attached to the other side of the SE pellet. For the Li deposition test below the in situ formed Ag-Li intermetallic layer (ALI), 26.7 mg of cathode composite (areal capacity =  $2.3 \text{ mAh cm}^{-2}$ ) was used to supply active Li, thus detecting a noticeable change in the anode thickness on the SS foil. All fabrication steps were conducted in an Ar-filled glove box and dry room at a dew point of approximately  $-70^\circ\text{C}$ . The cell tests were carried out using a battery cycler (WBCS3000L, WonAtech, Korea) at  $55^\circ\text{C}$ . For the cycling performance test, the galvanostatic charge/discharge modes were used at current densities of 0.2 and 0.5 C in the voltage range of 2.4 – 4.25 V vs.  $\text{Li/Li}^+$ . For the rate capability test, the unit cells were cycled at a charging rate of 0.2 C and different discharging rates from 0.2 to 14 C ( $1 \text{ C} = 180 \text{ mA g}^{-1}$ ), and thereafter, cycled at 0.2 C. In order to access the symmetric cell, the Ag-Li alloy or Li foil was attached to both sides of the SE pellet. Electrochemical impedance spectroscopy (EIS) analysis was performed in the frequency range of 10 mHz to 7 MHz at  $25^\circ\text{C}$  using a VSP tester (Biologic, France).<sup>[S1, S5-S7]</sup>

*Characterization:* To characterize the Ag-Li alloyed phase and morphological changes of the electrode during electrochemical tests, the cycled cells were disassembled in a glovebox; then, the pelleted electrodes were analyzed using an X-ray diffractometer (X'pert Pro, PANalytical, Netherlands) with  $\text{Cu K}_\alpha$  ( $\lambda = 0.15406 \text{ nm}$ ) and field-emission scanning electron microscopy (FE-SEM, S-4800, Hitachi, Japan). For the X-ray diffraction (XRD) analysis, a gastight XRD holder (PANalytical, Netherlands) was used to avoid air exposure. The elemental mapping of the electrodes was performed using energy-dispersive X-ray spectroscopy (EDS, Sirion, FEI, USA). The chemical compositions and bonding characteristics of the LPSCI surface were analyzed using X-ray photoelectron spectroscopy (XPS, K-alpha, Thermo Scientific, England) with an  $\text{Al K}_\alpha$  line as the X-ray source. The C 1s peak (284.8 eV) was used as reference. For the XPS characterization, we used 250  $\mu\text{m}$  thick Li for cell fabrication to easily detach the anode from the pelleted cell after electrochemical tests. A vacuum transfer module (Thermo Scientific, England) was used to avoid air contamination. X-ray microscopy (XRM,

Xradia 520 Versa, ZEISS, Germany) with a source voltage of 80 kV and a power of 7 W using the Air filter was employed to analyze the internal interfacial morphology of the electrode without cell fracture. A 4× objective was used with an exposure of 3 s and 2401 projections, giving a resolution of about 0.8408  $\mu\text{m}$ .

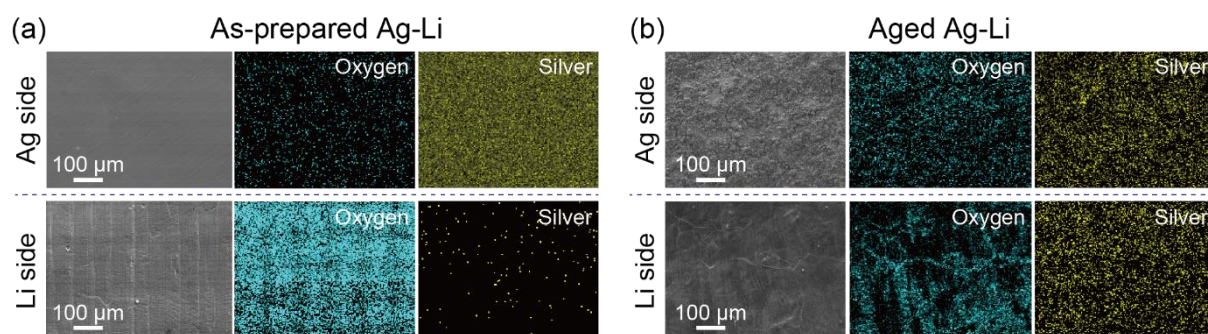


**Figure S1.** Top-view SEM images of the as-prepared Ag-Li and aged Ag-Li alloys along with EDS elemental mapping images of oxygen and silver.

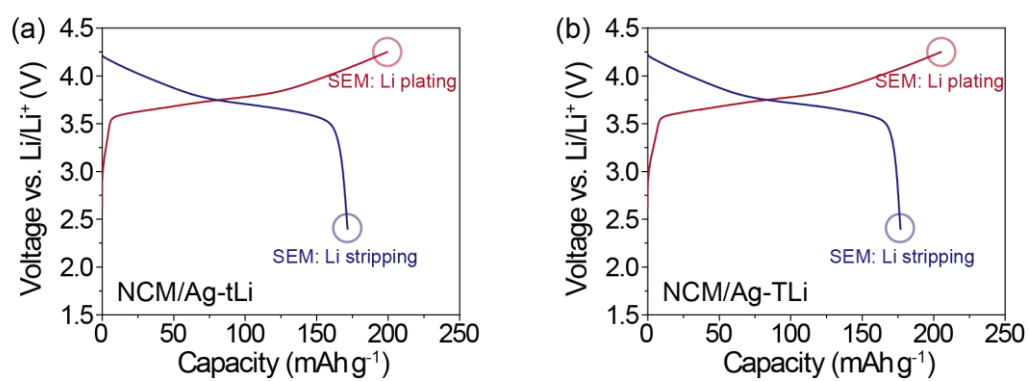


**Figure S2.** The 1st voltage profiles of the NCM/Ag-tLi and NCM/Ag-TLi cells at 0.2 C for the SEM analysis shown in Figures 2a and c.

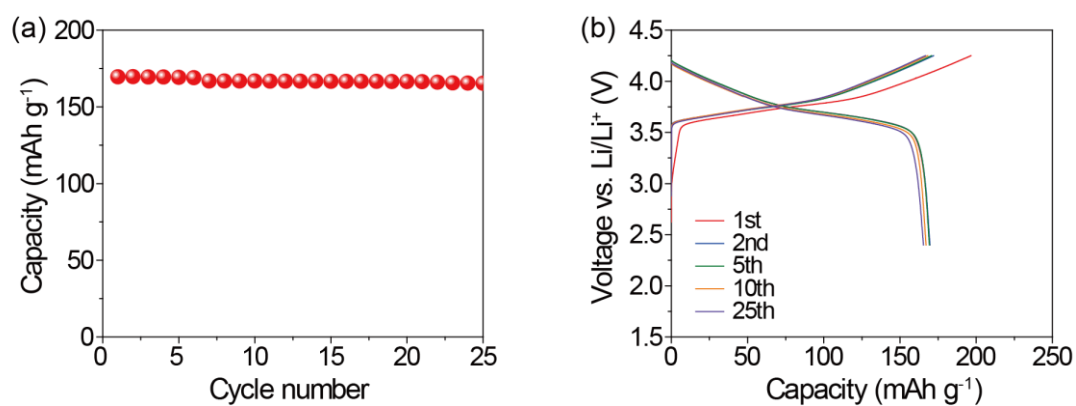


**Figure S3.** (a) Cycling performance and (b) corresponding voltage profiles of the NCM/Ag-tLi cells at 0.2 C.

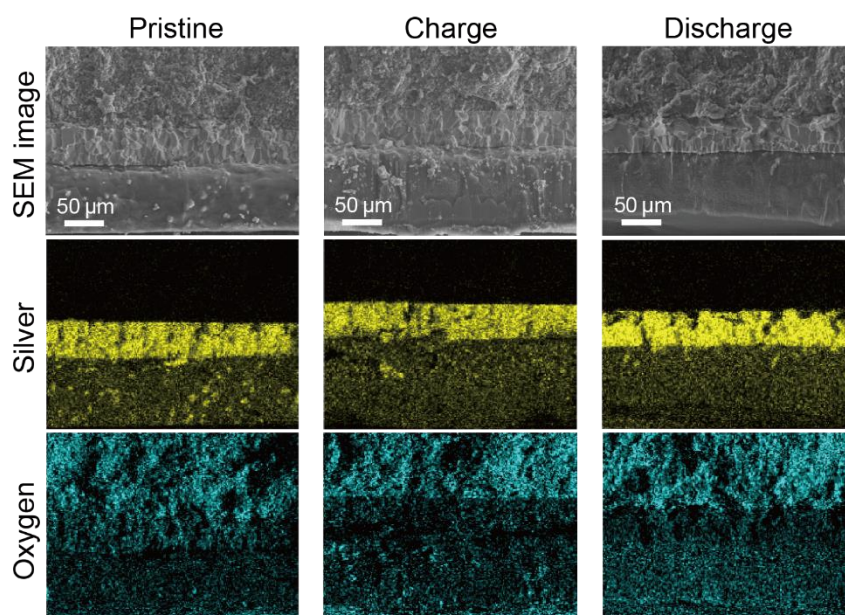


**Figure S4.** Cross-sectional SEM images of the NCM/Ag-Li cells along with EDS elemental mappings of silver and oxygen during the 1st cycle shown in Figure 2c.

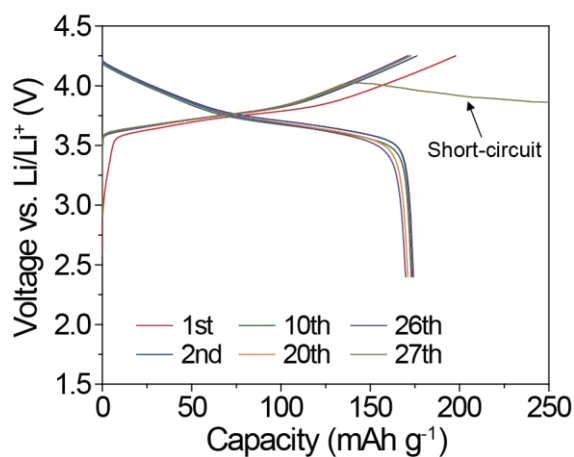


**Figure S5.** Voltage profiles of the NCM/Li cell shown in Figure 2d.

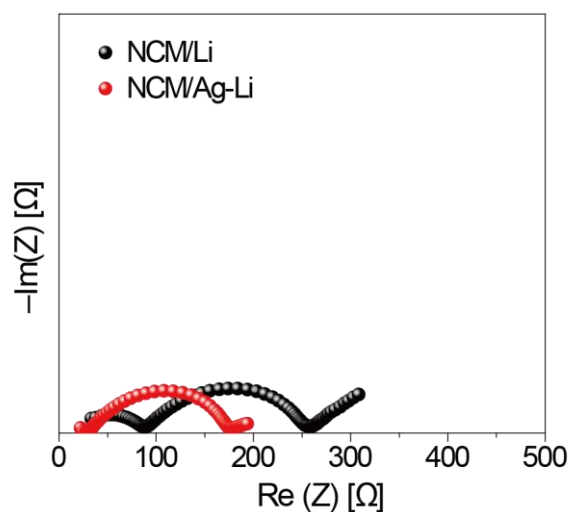


**Figure S6.** Overlapped EIS spectra of NCM/Li and NCM/Ag-Li cells at the 25th charged state during rate performance test shown in Figure 2f, showing a smaller resistance for the NCM/Ag-Li cell compared to the NCM/Li cell. This confirms the stable SE/Ag-Li interface at high current densities.



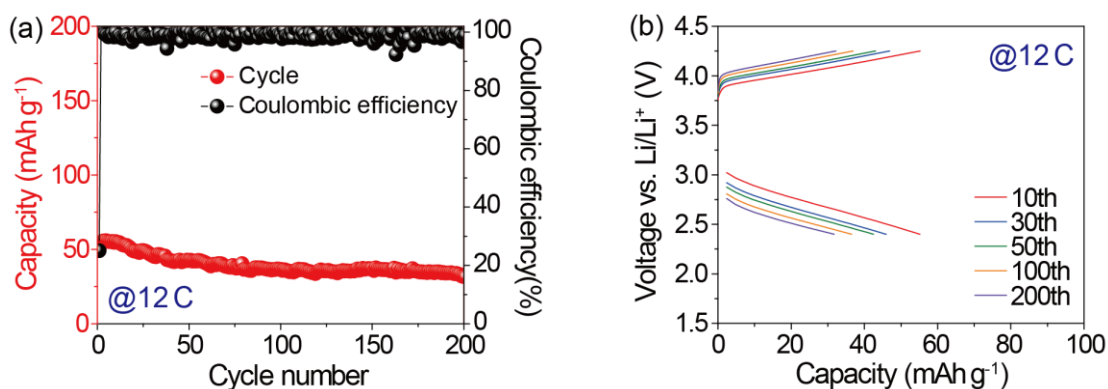


**Figure S7.** (a) Cycling performance and corresponding coulombic efficiency of the NCM/Ag-Li cell at 12 C, and (b) their corresponding voltage profiles. To generate a stable interface in the cell, the cell was precycled at a charging rate of 0.2 C and a discharging rate of 12 C at the first cycle.

Note: The initial CE is low because the charge capacity at 0.2 C is much higher than that of the discharge capacity at 12 C due to the large discharging overpotential during the precycling process to form a stable interface in the cell. In addition, side reactions that occur during the first charging process can affect the low initial CE.<sup>[S3,S8]</sup>

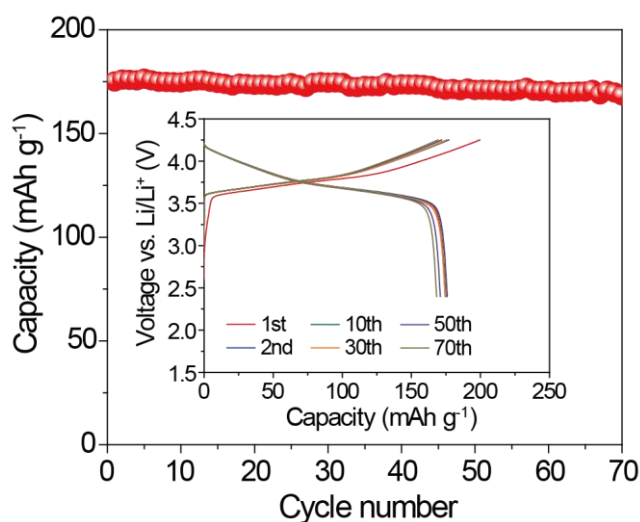


**Figure S8.** Cycling performance and (inset) corresponding voltage profiles of the NCM/Ag-Li cell with a practical-loading density of 24 mg<sub>NCM</sub> cm<sup>-2</sup> at 0.2 C.

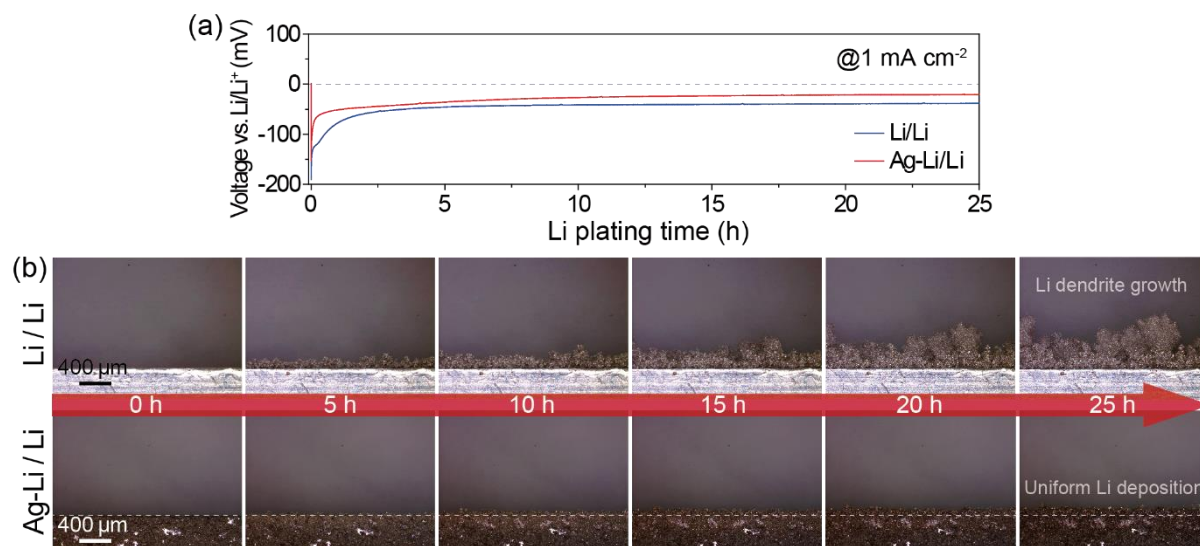


**Figure S9.** (a) Voltage profile of the Li/Li symmetric and Ag-Li/Li cells during Li plating at  $1 \text{ mA cm}^{-2}$ , and (b) corresponding optical microscope images of the Li/Li symmetric and Ag-Li/Li cells taken at various times during Li deposition.

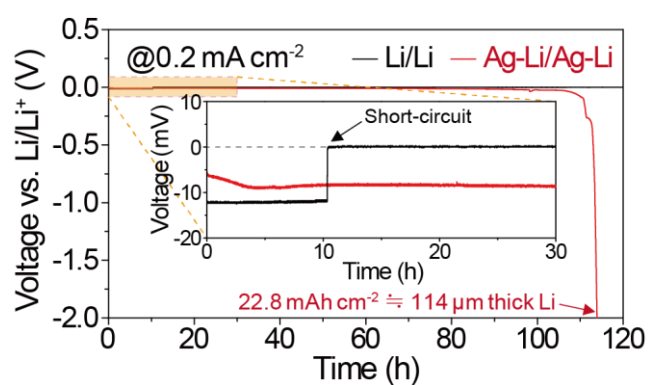


**Figure S10.** Voltage profiles of the Li/Li and Ag-Li/Ag-Li symmetric cells at  $0.2 \text{ mA cm}^{-2}$  during long-lasting Li plating. For this test,  $150 \mu\text{m}$  thick Li was used to fabricate the Ag-Li alloy.

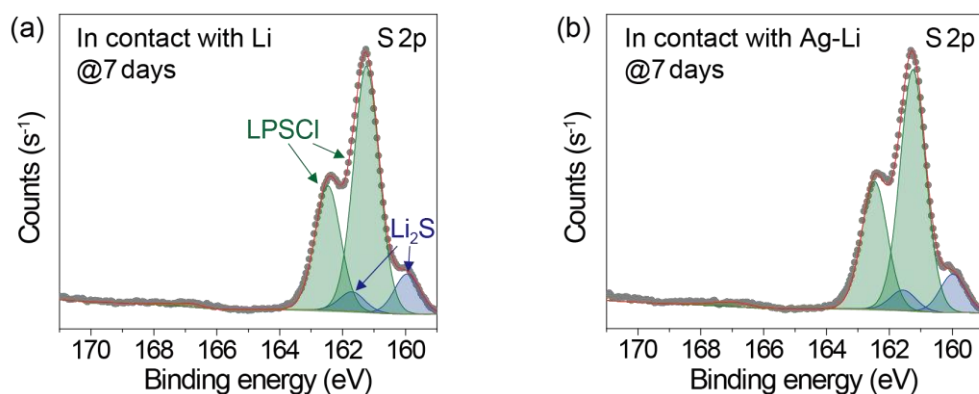


**Figure S11.** S 2p XPS spectra of the LPSCI in contact with the (a) Li metal and (b) Ag-Li alloy after 7 days.

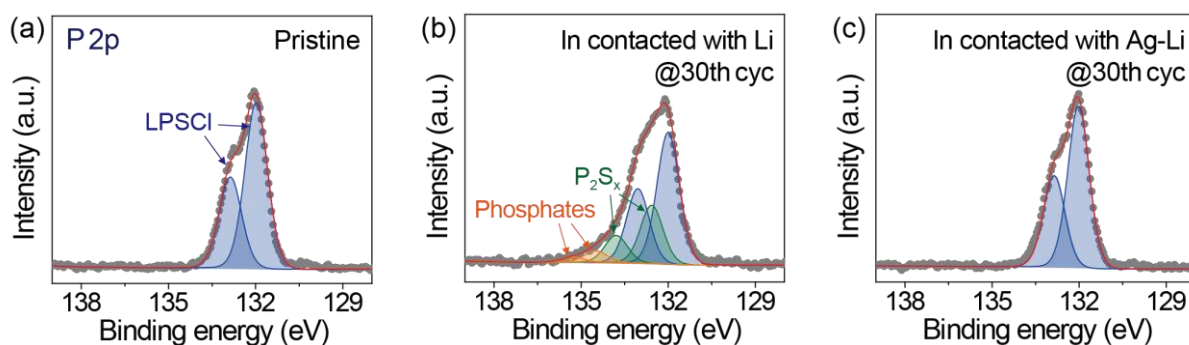


**Figure S12.** P 2p XPS spectra of the (a) pristine LPSCI, (b) LPSCI in contact with Li, and (c) LPSCI in contact with Ag-Li after 30 cycles. The LPSCI of Li cell exhibits the decomposition products such as P<sub>2</sub>S<sub>x</sub> and phosphates,<sup>[S3,S9]</sup> resulting from the interfacial side reactions.

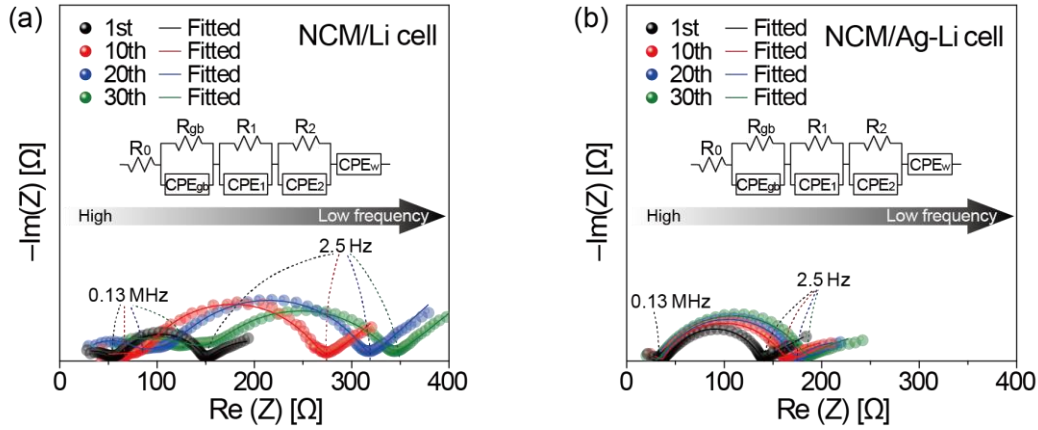


**Figure S13.** Nyquist plots for the (a) NCM/Li and (b) NCM/Ag-Li cells shown in Figure 2d. The NCM/Ag-Li cell showed smaller resistances than those of NCM/Li cell at the charged state during 30 cycles, supporting the stable interface at the anode side as shown in Figure 3k. The inset indicates an equivalent circuit model.<sup>[S10,S11]</sup> ( $R_0$ : SE resistance.  $R_{gb}$ : Grain boundary resistance of the SE.  $R_1$  and  $R_2$ : Charge transfer resistance at the cathode and anode interfaces, respectively.  $CPE_1$  and  $CPE_2$ : Constant phase elements at the cathode and anode side, respectively.  $CPE_w$ : Warburg element, indicating the solid-state diffusion process of  $Li^+$  in the NCM particles)

Note: To further demonstrate the interfacial stability of the ALI to the sulfide-based SE, EIS tests were carried out over 30 cycles. Figure S13 displays the EIS spectra of Li and Ag-Li cells at 25 °C. The combined semicircle in the high- and middle-frequency regions is attributed to the small grain boundary resistance of the SE ( $R_{gb}$ ) and large cathode/SE interfacial resistance ( $R_1$ ), respectively. The semicircle in the low-frequency region is correlated with the charge transfer resistance between the anode and SE ( $R_2$ ). The x-axis intercept is assigned to the resistance of the SE layer ( $R_0$ ), which corresponds to the bulk resistance of the SE. While the Li cell showed a conspicuous increase in impedance, a small increase in impedance was observed in the Ag-Li cell. Considering the cathode and SE are the same in the Li and Ag-Li cells, in the low-frequency region, the result of the Li cell is mainly due to the increase in the resistance caused by the interfacial side reactions at the anode/SE interface, and the Ag-Li cell exhibited a relatively small increase in resistance because it maintained a stable anode interface during cycling. This spectroscopic result supports the interfacial stability at the anode side in the Ag-Li cell.

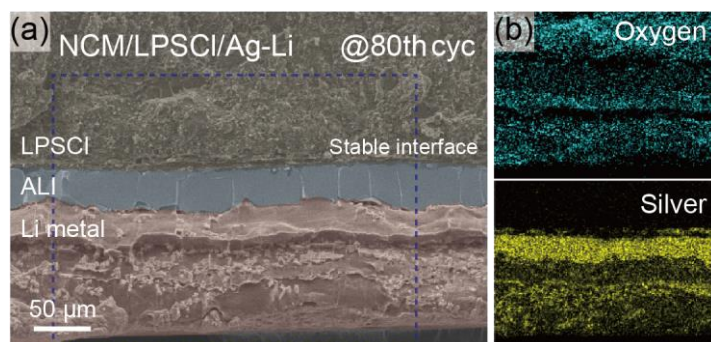


**Figure S14.** (a) Cross-sectional SEM image of the NCM cell with Ag-Li alloy anode after 80 cycles and (b) corresponding EDS elemental mappings of oxygen and silver from the inset blue box in (a).

## References

- [S1] S. W. Park, G. Oh, J.-W. Park, Y.-C. Ha, S.-M. Lee, S. Y. Yoon, B. G. Kim, *Small* **2019**, *15*, 1900235.
- [S2] S. Boulineau, M. Courty, J.-M. Tarascon, V. Viallet, *Solid State Ion.* **2012**, *221*, 1.
- [S3] J. Auvergniot, A. Cassel, J.-B. Ledeuil, V. Viallet, V. Seznec, R. Dedryvère, *Chem. Mater.* **2017**, *29*, 3883.
- [S4] A. D. Bui, S.-H. Choi, H. Choi, Y.-J. Lee, C.-H. Doh, J.-W. Park, B. G. Kim, W.-J. Lee, S.-M. Lee, Y.-C. Ha, *ACS Appl. Energy Mater.* **2021**, *4*, 1.
- [S5] K. H. Park, D. W. Kang, J.-W. Park, J.-H. Choi, S.-J. Hong, S. H. Song, S.-M. Lee, J. Moon, B. G. Kim, *J. Mater. Chem. A* **2021**, *9*, 1822.
- [S6] D. W. Kang, J. Moon, H.-Y. Choi, H.-C. Shin, B. G. Kim, *J. Power Sources* **2021**, *490*, 229504.
- [S7] B. G. Kim, C. Jo, J. Shin, Y. Mun, J. Lee, J. W. Choi, *ACS Nano* **2017**, *11*, 1736.
- [S8] D. H. S. Tan, E. A. Wu, H. Nguyen, Z. Chen, M. A. T. Marple, J.-M. Doux, X. Wang, H. Yang, A. Banerjee, Y. S. Meng, *ACS Energy Lett.* **2019**, *4*, 2418.
- [S9] J. Auvergniot, A. Cassel, D. Foix, V. Viallet, V. Seznec, R. Dedryvère, *Solid State Ion.* **2017**, *300*, 78.
- [S10] W. Zhang, D. A. Weber, H. Weigand, T. Arlt, I. Manke, D. Schröder, R. Koerver, T. Leichtweiss, P. Hartmann, W. G. Zeier, J. Janek, *ACS Appl. Mater. Interf.* **2017**, *9*, 17835.
- [S11] R. Koerver, I. Aygün, T. Leichtweiß, C. Dietrich, W. Zhang, J. O. Binder, P. Hartmann, W. G. Zeier, J. Janek, *Chem. Mater.* **2017**, *29*, 5574.